ELSEVIER

Pull-Out Behavior of Corrugated Steel Fibers

Qualitative and Statistical Analysis

Gilles Chanvillard* and Pierre-Claude Aïtcin†
**ENTPE Département Génie Civil et Batiment, URA CNRS 1652, Vaulx en Velin, France and*
†Université de Sherbrooke, Département Génie Civil, Sherbrooke, Canada

The choice of a steel fiber to reinforce a cementitious matrix is often made with a misunderstanding of the real capabilities of the steel fiber. In spite of the sophisticated approaches in the case of straight steel fibers, the behavior of nonstraight fibers is much less understood. A very simple test, the pull-out test, allows us to evaluate these capabilities. An experimental program is presented that has investigated the effect of the length and orientation of a corrugated circular cross-section steel fiber anchored in different water to cement (w/c) ratio matrices with a new apparatus allowing one to pull-out any variety of steel fiber from concrete matrices. The analysis of the experimental results is at first qualitative and then statistical to objectively identify the significant parameters on the fiber pull-out behavior. Because w/c ratio appears to govern the failure mode, that is fracture or debonding of the fiber, it has only a slight effect on the fiber slipping behavior. In case of debonding, the fiber slips into the print of its initial geometry with minor matrix internal degradations and is straightened after complete extraction, dissipating a significant amount of cold work energy. Finally, length and orientation of the fiber interact and considerably affect the debonding behavior. In particular, a local matrix crushing in the crack plane delays the fiber mobilization by local unfolding. ADVANCED CEMENT BASED MATERIALS 1996, 4, 28–41

KEY WORDS: Bearing, Cement matrix, Crushing, Debonding, Energy, Friction, Pull-out behavior, Pull-out test, Steel fibers

Steel fibers are used in a concrete matrix to reduce cracking problems and concrete brittleness, energy being dissipated within the fissured surfaces. The addition of fibers a few centimeters long does not result in a significant increase of concrete mechanical properties before failure, however the benefits of adding steel fiber to concrete become evident when looking at the postfailure behavior. Depending on the amount of steel fibers that has been used, concrete becomes a more or less pseudoductile material [1,2].

The first steel fibers used in concrete were straight ones. Analytical models were developed to explain their beneficial action on concrete matrices [3,4]. The behavior of a steel fiber across a crack was found to be somewhat complex. A straight fiber acting in the direction of the load essentially develops bound stresses at its interface with the hydrated cement paste. During its pull-out, stress evolves from an elastic behavior to a frictional one [5–9]. If the fiber is not in the direction of the stress, the fiber is bent in the crack plane, developing plastic deformation so that the necessary energy is increased [6,10,11].

Over the years, so-called improved shaped fibers have been brought onto the market by different fiber producers. Such fibers are supposed to out-perform straight fibers in improving fiber-reinforced concrete properties. It must be admitted that sometimes it is difficult to find any scientific or technological support for this statement. It is evident that this type of fiber must behave quite differently than a straight fiber. In some cases, such fiber has a nonuniform cross-section area and acts like a microdeformed reinforcing bar that presents stress concentrations at each indentation. When the fiber is made of a deformed hot or cold drawn wire, it can be straightened during its pull-out so that it is necessary to take into account the corresponding plastification energy to understand its behavior [12–15].

As for straight fibers, the orientation of a nonstraight fiber influences the behavior of a steel fiber-reinforced concrete in which the fibers are statistically dispersed, therefore the experimental study of nonstraight fiber becomes quite complex.

Address correspondence to: Dr. Gilles Chanvillard, Dépt Génie Civil et Batiment, ENTPE, URA CNRS 1652, 69518 Vaulx et Velin, France.
Received February 20, 1995; Accepted November 8, 1995

ISSN 1065-7355/96/$15.00
PII S1065-7355(96)00036-3

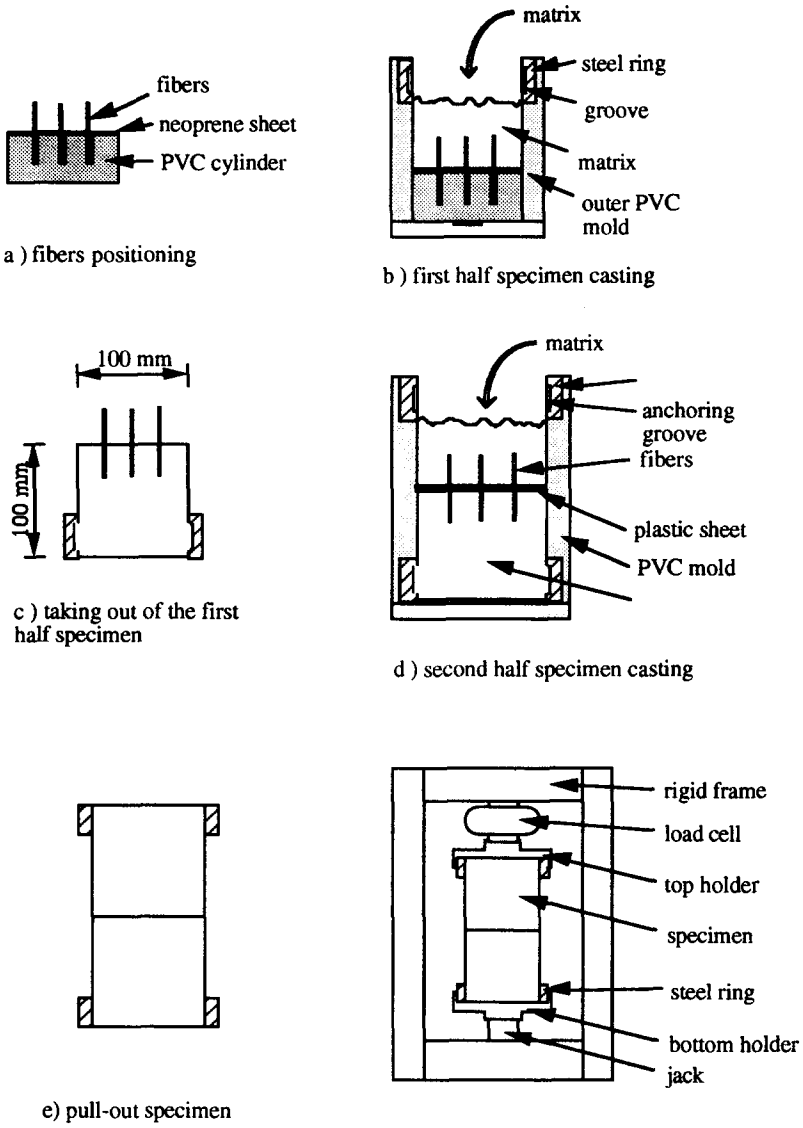

FIGURE 1. Casting of the specimen and experimental apparatus.

To develop a better understanding of the behavior of nonstraight fibers in cementitious matrices, we present an extensive experimental program on the influence of the fiber length, its orientation with respect to the cracked plane, and the water to cement (w/c) ratio of the matrix in the case of a corrugated fiber. Because the possible interaction of the mechanical anchorage of the fiber with the aggregate phase of the matrix has to be taken into consideration, this study has been carried out directly on a microconcrete rather than on a paste or a mortar.

In the first part of this presentation, the analysis of experimental results will be qualitative in order to better explain the failure mechanism when an individual steel fiber is pulled out of a concrete matrix. In the second part, experimental results will be analyzed statistically in order to find the significance of the three selected parameters on the behavior of corrugated steel fibers in concrete matrices. This approach of an individual fiber behavior may be used for any type of steel fiber to identify the significant parameters.

TABLE 1. Concrete composition for each water to cement (w/c) ratio

	w/c		
Composition	**0.30**	**0.50**	**0.70**
Water (L/m^3)	170	222	230
Cement (type I) (kg/m^3)	585	444	328
Sand (kg/m^3)	790	795	875
Aggregate 5 mm (kg/m^3)	930	935	935
Superplasticizer (L/m^3)	13.9	0	0
Compressive strength (MPa)	78	49	29

TABLE 2. Frequency of pull-out mode by debonding

	45° angle			90° angle		
w/c	One wave	Two waves	Three waves	One wave	Two waves	Three waves
0.30	100%	100%	50%	100%	83%	8%
0.50	100%	100%	75%	100%	100%	8%
0.70	100%	100%	83%	100%	100%	25%

Experimental Program

Selection of the Fiber

To simplify this experimental study, we decided to select a nonstraight fiber having at the same time a regular shape that could be easily modeled mathematically for further theoretical developments. This consideration led to the choice of a fiber made of corrugated cold drawn wire having a circular cross-section area.

The corrugated shape results in mechanical anchorage distributed all alone the fiber. Depending on the number of waves that are embedded in the matrix on each side of the crack, it is possible to study the effect of the fiber anchor length.

Experimental Apparatus

To conduct this experimental study, we decided to develop an experimental model based on an idealized pull-out test. Following a critical review of the previous apparatus found in the literature, we decided to conceive a model having the following characteristics [16–18]:

- the fabrication of the specimens should be simple to limit their variability;
- the fibers should be precisely located, oriented, and held with respect to the crack during the casting of the specimens;
- the anchored length of the fibers could be varied as well as the orientation of the fibers;
- external stress concentrations should be minimized during the pull-out test;
- the use of a concrete matrix rather than a mortar or a paste matrix should be favored as previously mentioned; and
- the selected apparatus should allow the casting of a 100 × 200-mm samples.

A particular apparatus complying to all these requirements was developed [19,20]. The specimens are cast into two main stages (Figure 1). In the first stage, the fibers (one or more) are placed into a PVC cylinder. This cylinder has holes that allow an accurate positioning of the fibers as far as embedded length and angle are concerned. With the use of this cylinder, the fibers are well secured during the casting of the specimen. To avoid any slurry infiltration inside the cylinder holes, a neoprene sheet is pierced by the fibers, which ensure the sealing. Then, the outer mold of the first half specimen is fixed. On the upper part of this mold, a steel ring is screwed on, which will allow us to fix the specimen on the set-up for the test. Note that a few millimeters deep groove allows us to develop a good anchorage between the matrix and the steel ring. The first half specimen is finished after casting the cementitious matrix. In the second stage, after 24 h, the mold is removed. The conception of this mold with half cylinders makes this step very easy and safe for the specimen. The fibers protrude over the expected embedded length from the half specimen. Then a plastic sheet is placed on the crack plane to prevent any bond between the two half-specimens. Another outer mold is fixed with a steel ring on the upper part. Note that the molds must be very well machined to ensure coaxiality between the

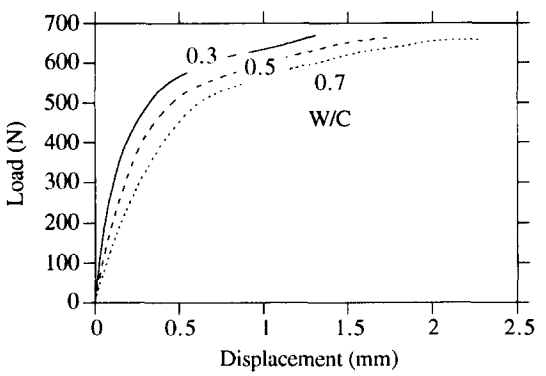

FIGURE 2. Load-displacement curves for a failed fiber (orientation = 90°, three-waves-long fiber).

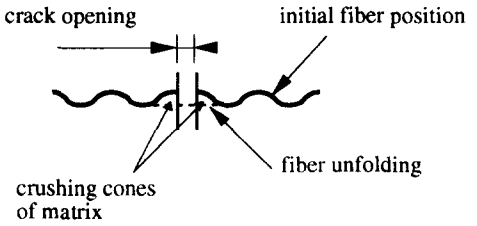

FIGURE 3. Crushing matrix cones and local fiber unfolding in case of perpendicular fiber.

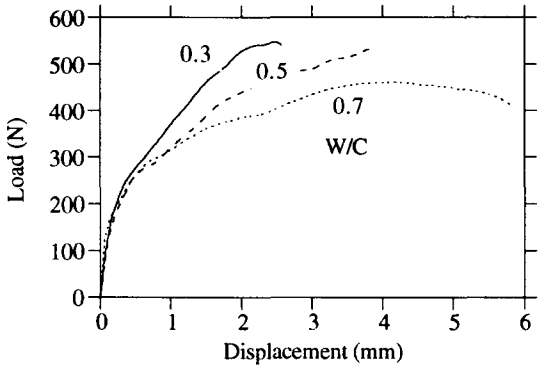

FIGURE 4. Load-displacement curves for a failed fiber (orientation = 45°, three-waves-long fiber).

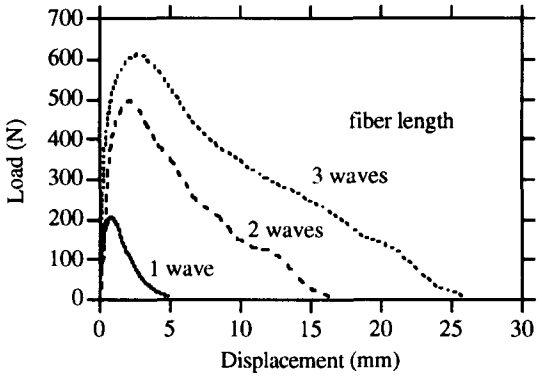

FIGURE 6. Load-displacement curves in case of fiber debonding (w/c = 0.7, orientation = 90°).

two steel rings. The matrix is poured and the mold is removed after 24 h. The finished specimen can then be cured in different conditions until testing.

Studied Parameter

With this particular apparatus, it has been possible to study the effect of the fiber length corresponding to one, two, and three anchored waves.

The second parameter that has been under study is the w/c ratio of the concrete. Three values were selected: 0.30 that corresponds to a high performance concrete, 0.50 that corresponds to normal strength concrete, and 0.70 that corresponds to weak concrete. These concretes were made with a small coarse aggregate (D_{max} = 5 mm). Their composition is given in Table 1 as well as their 28d compressive strength measured on 100 × 200-mm specimens.

Finally, two fiber orientations were considered: one perpendicular to the cracked plane and the other making a 45° angle with this plane.

Experimental Conditions

Three specimens were cast for each of these 18 configurations. Moreover each specimen contained three fibers having the same length and orientation. A data acquisition system automatically recorded the load and displacement values that corresponded to the average for the three fibers.

The reproducibility of the experimental apparatus was checked by testing a particular configuration, at the beginning and at the end of the experimental series [20].

Experimental Results

As previously explained, the experimental results will be discussed at two levels. On a qualitative basis, the behavior of the fibers will be discussed based on the shape and the relative position of the load-displacement curves obtained for different configuration. On a quantitative basis, the pull-out behavior will be studied as a function of different parameter using a factorial statistical analysis according to a method presented in the Appendix.

Two types of failure were observed during the ex-

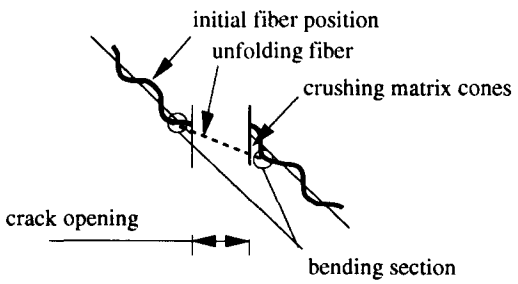

FIGURE 5. Crushing matrix cones and local fiber unfolding in case of 45° inclined fiber.

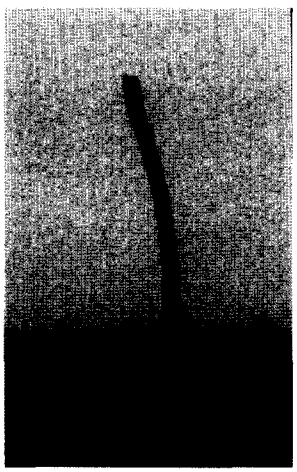

FIGURE 7. Two-waves fiber after extraction.

Advn Cem Bas Mat
1996;4:28–41

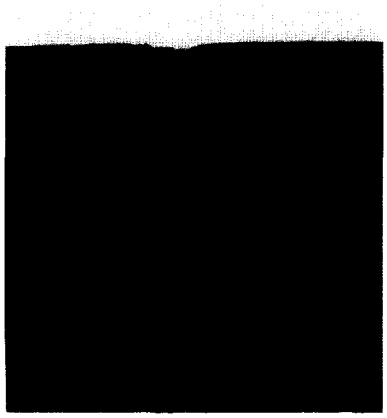

FIGURE 8. Mark left by the fiber of Figure 7.

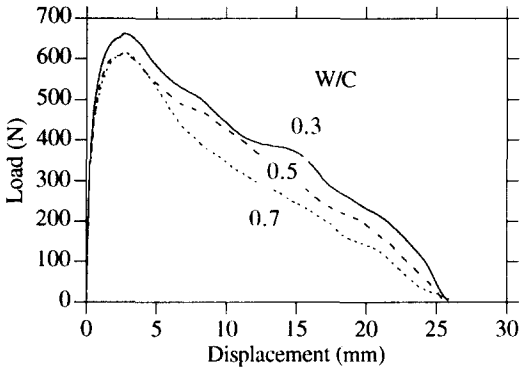

FIGURE 10. Influence of the w/c ratio on the load-displacement curves (orientation = 90°, three-waves-long fibers).

periments: either fibers were debonded then slipped until there were completely pulled out, or they were broken before being pulled out from the matrix. Table 2 presents the proportion of debonded fibers for each configuration.

When the fibers had only one or two waves embedded on each side of the crack, they were pulled out almost all the time whatever their orientation or w/c ratio. On the contrary, when the fibers were three waves long, most of them were broken before being debonded when perpendicular to the cracked plane. A similar conclusion was drawn by Banthia [12]. When the fibers were at a 45° angle, most of them were pulled out from the weaker concrete (w/c = 0.70), whereas only half of them were pulled out from the strongest matrix (w/c = 0.30).

Qualitative Analysis

FAILURE MODE. Figure 2 presents the load-displacement curves for the three values of the w/c ratio in case of a three-waves-long fiber perpendicular to the failure line. It is seen that the shape of the three curves is about the same. These are composed of a first step ascending part that curves until a maximum load is recorded. Throughout this process, the fiber works exclusively in traction with plastic deformations and necking. The recorded load at failure was equal to about 660 N in all cases. This load corresponds to a stress of 1160 MPa when the fiber breaks. This maximum stress value agrees closely with the one given for the steel in the manufacturer's data sheet (1200 MPa).

The displacement measured at failure increases with the w/c ratio. This phenomenon can be explained by the size of the matrix cone that is crushed on each side of the crack when failure occurs as shown in Figure 3 [11,21]. The existence of these cones concurs with observations made by other scientists. When the w/c ratio is high, the size of the cone is bigger so that the local straightening of the fiber is greater. The displacements measured at failure varied between 1.5 and 2 mm, corresponding to the sum of three components—an elastic and a plastic deformation of the steel to which the local straightening of the fiber must be added.

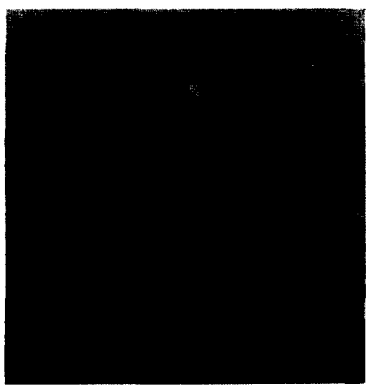

FIGURE 9. Matrix crushing in the crack plane.

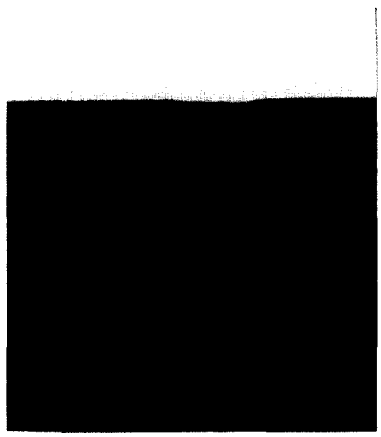

FIGURE 11. Mark and crushing for a one-wave fiber.

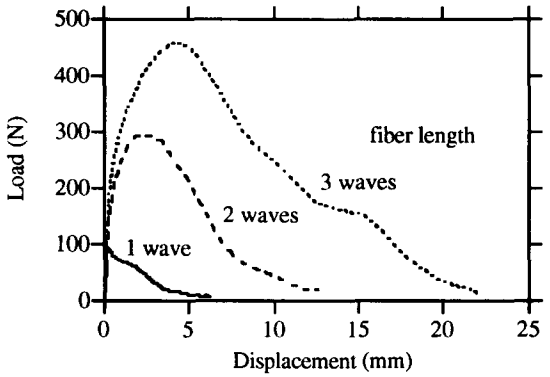

FIGURE 12. Influence of the fiber length on the load-displacement curves (orientation = 45°, w/c = 0.7).

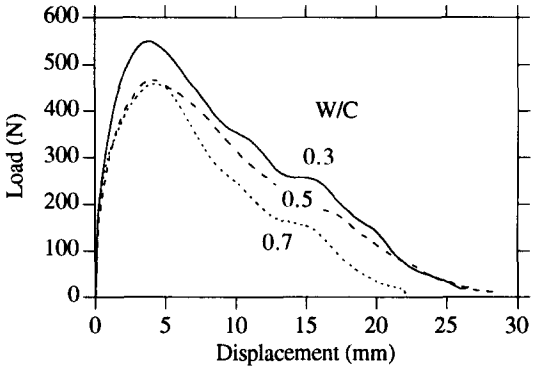

FIGURE 14. Influence of the w/c ratio on the load-displacement curves (orientation = 45°, three-wave-long fibers).

When the fibers are at a 45° orientation, fewer fibers fail by direct tensile stress as shown in Table 2. Figure 4 presents the results obtained for the three lengths and the three w/c ratios in case of a fiber that is three waves long. As in the preceding case, the load-displacement curves can be decomposed in three main parts. However, failure occurs at a lower load 500 N, which corresponds to a 880 MPa stress in the steel.

This lower stress at the point of failure is a consequence of the mode of failure of the fiber that occurs in this case as a combination of traction and flexion. Traction occurs during the pull-out, whereas the flexion mode occurs during the opening of the crack. This last mode results from the orientation of the fiber with respect to the crack and from the fiber shape.

The crushing of two cones on each side of the crack plane produces a more pronounced straightening of the fiber when the fiber is oriented at 45°. Because the testing machine ensures the parallelism between the two planes of the crack, the fibers were solicited in flexion (Figure 5). It was also noticed that the failure of the fiber occurred always at the top of a wave where steel had been weakened during the manufacturing process in this area of maximum curvature.

FAILURE BY DEBONDING. Debonding was the most frequent mode of failure for the one- and two- waves-long fibers. This mode of failure corresponds to the debonding of the fiber followed by its slipping along its initial print until it is finally pulled out. The load displacement curves have always been about the same shape. First of all, they present a very steep part before a maximum load is recorded for a displacement of some millimeters. This peak is followed by a progressive decrease of the sustained load until it reaches a zero value corresponding to the complete pull-out of the three fibers.

Figure 6 presents the results obtained for a long fiber (three waves) cast in the weakest concrete (w/c = 0.70). It has been selected because it best illustrates this case. The pull-out of the fiber could have occurred according to two extreme modes. First mode, fibers could have kept their corrugated shape during the process so that the matrix would have been completely destroyed in the fiber area during the pull-out process. Second mode, if the matrix was not altered, the fiber was continuously deformed during its slipping until its final pull-out within its initial print. Figure 7 shows the shape of a

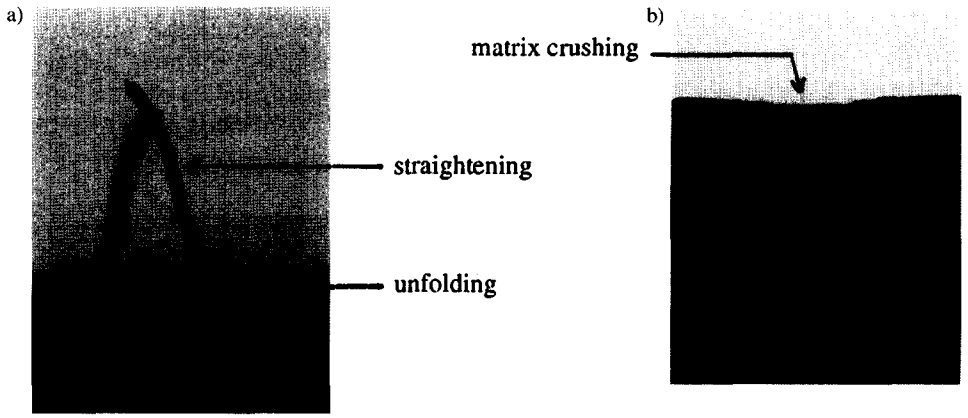

FIGURE 13. (a) Two-waves inclined fiber after extraction. (b) Mark left by the fiber of Figure 13a.

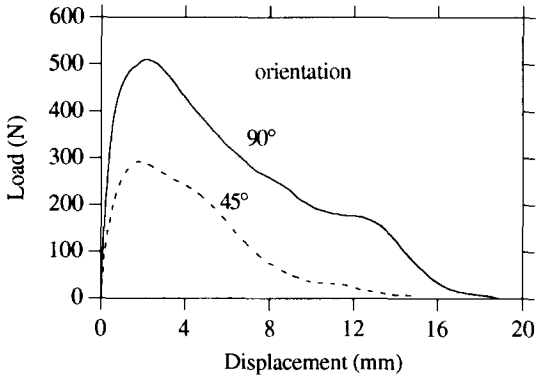

FIGURE 15. Influence of the fiber orientation (w/c = 0.5, two-waves-long fibers).

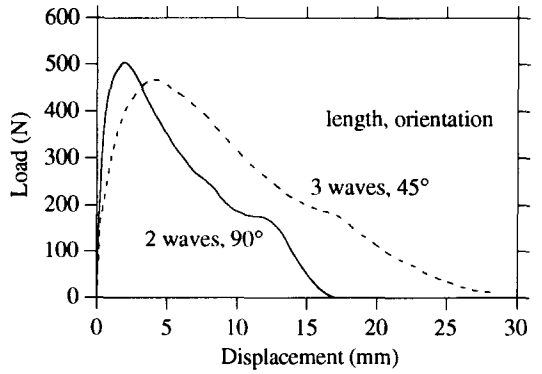

FIGURE 16. Length-orientation interaction on the fiber load-displacement curves (w/c = 0.5).

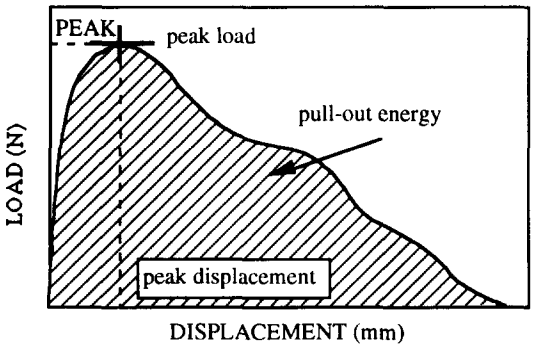

FIGURE 17. Defined parameter to characterize the fiber pull-out behavior.

two-waves-long fiber after its pull-out. It has lost its corrugated shape; it is almost straight. To figure out how damaged the matrix along the fiber print could be, we carefully cut a specimen along a print and polished until the print could be observed as shown in Figure 8. It is seen that the matrix was not damaged at all during the slipping process, even in the case of the weakest concrete. The observation of the print surface under optical microscopy did not reveal any more serious damages. Only some polishing action by the fiber during its pull-out could be observed. The same results were obtained by Banthia [21].

Following these observations, it is possible to propose the following failure mechanism. First, the pull-out behavior is elastic and is perfectly reversible. The deformations of the fiber and of the matrix are compatible. Second, the increase of the load results in the early failure of a small cone on both sides of the crack. The shape and size of these cones vary according to the strength of the concrete and the level of the load applied, which is in turn related to the length of the embedded fiber. It is possible that the fiber is not totally debonded when the failure of the small cones occurs (Figure 9).

The fiber becomes totally free over the few millimeters depth of the cones. Following an increase of the sustained load, it can be unfolded and straightened. Simultaneously, the fiber becomes progressively debonded from the matrix all along its print. During this phase, displacements of several tenths of millimeters occur at the level of the cracked plane while the anchored end has not yet started to move.

Finally, the fiber reaches a state where it is totally debonded and each of its sections moves during the pull-out process. The fiber slips into its print, each of its parts having a curvature that varies continuously within the fiber, dissipating a significant amount of cold work energy. It is the only mechanism that can explain the straightening of the fiber after its final pull-out. The curvature observed on the straightened fiber (Figure 7) results from the release of elastic stresses that develops a residual strain. This type of mechanism can be qualified as bearing or mechanical anchorage.

Consequently, taking into account the major role played by the plastic deformation of the steel during all the slipping process, the maximum load that can be supported by the fiber can be reached after the fiber

TABLE 3. Displacement (mm) at the peak load values

	45° angle			90° angle		
w/c	One wave	Two waves	Three waves	One wave	Two waves	Three waves
0.3	0.27	1.95	3.35	0.62	1.32	1.87
0.5	0.44	1.56	4.27	0.74	1.56	1.97
0.7	0.17	1.87	4.37	0.78	1.95	2.05

TABLE 4. Analysis of variance on displacement at the peak load values

Source	df	Sum of squares	Mean square	*F* value	*p* value
w/c	2	.280	.140	1.412	.3436
Length	2	18.408	9.204	92.754	.0004
Angle	1	1.614	1.614	16.265	.0157
w/c × length	4	.298	.074	.750	.6062
w/c × angle	2	.012	.006	.059	.9433
Length × angle	2	4.903	2.451	24.703	.0056
Residual	4	.397	.099		

Dependent variable is peak displacement. df = degrees of freedom.

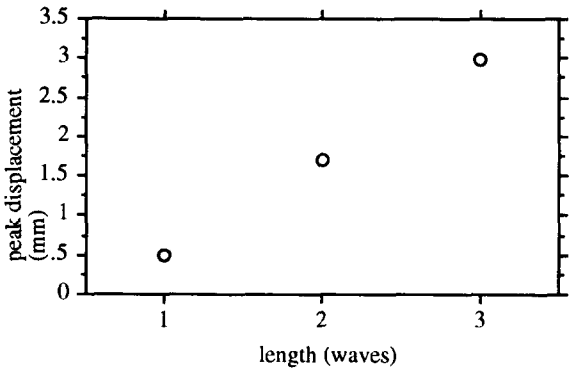

FIGURE 18. Influence of the fiber length on the peak load displacement.

starts to slip within its print and not necessarily at the time when it is totally debonded.

Moreover, during the pull-out process, some friction develops along the initial print at the fiber/matrix interface. Figure 10 illustrates the effect of the w/c ratio. The matrix seems to play a secondary role during the slipping process when compared to the mechanical anchorage, while it plays a more significant role on the maximum value reached at the peak load, which governs the failure mode.

Finally, in the case of a one-wave-long fiber, the cone crush annihilates the effect of the geometry of the fiber that can be pulled out with a minimum of plastic deformation (Figure 11).

To conclude, it is important to clearly differentiate between the friction and the bearing action. Friction is developed along the initial print of the fiber. Bearing action results from the fiber geometry, which must be continuously deformed to be pulled out.

Figure 12 presents the results obtained for different fiber lengths for a 0.70 w/c ratio concrete and 45° orientation. Here, too, it is seen that the length of the fiber is a very important parameter. Figure 13a illustrates the shape of a two-waves-long fiber after its pull-out, and Figure 13b illustrates the shape of the print left by this fiber within the matrix. The behavior of inclined fibers closely resembles that of perpendicular ones. However, due to its orientation, the fiber is unfolded on a greater length. As in the preceding case, the fiber starts to be debonded and slips within its print.

The straightening process occurs in two modes: the straightening by unfolding along the length freed by the cones, and the straightening by wire-drawing or unshaping during the slipping within the print, which results in the plastic deformation of the steel in each section. The shape of the fiber in Figure 13a clearly illustrates the difference between these two modes of straightening and their respective action. In this case, also, the behavior of the one-wave-long fiber is a limit case more difficult to explain. As far as the role of the matrix is concerned, it seems that in this case the w/c ratio does not play a significant role during the slipping of the fiber (Figure 14).

Figure 15 presents the results obtained for a w/c ratio of 0.50 for a two-waves-long fiber for a 90° and 45° orientation. It was observed that the sustained load is always greater when the fiber is perpendicular to the crack. These results do not agree with those presented

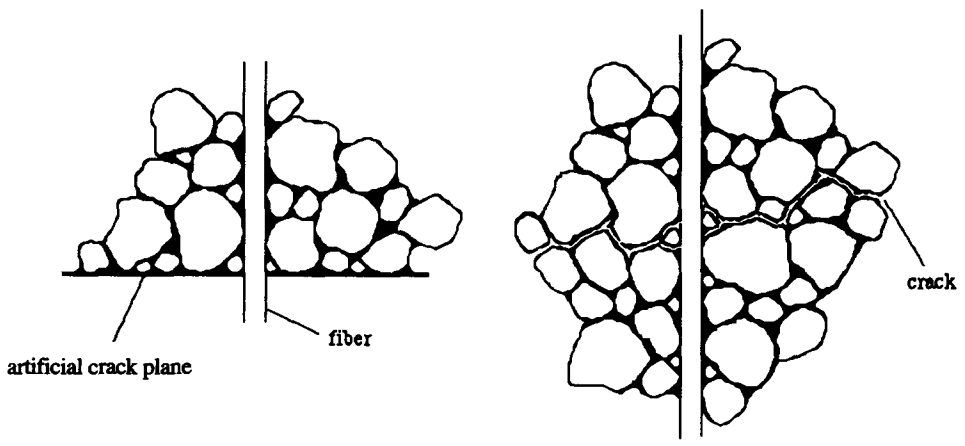

FIGURE 19. Schematic illustration of the surface effect in the crack plane.

TABLE 5. Peak load values (N)

	45° angle			90° angle		
w/c	One wave	Two waves	Three waves	One wave	Two waves	Three waves
0.3	134	372	568	301	574	689
0.5	104	312	485	235	527	650
0.7	105	300	473	213	518	647

by Naaman who obtained similar loads whatever the orientation of the fiber was [11]. This discrepancy can be related to the size of the cone, which should have been smaller in Naaman's paste matrix, and to the shape of the fiber (Naaman used straight fibers).

The size of the cone has been observed to be always greater when the fiber is inclined rather than perpendicular. The recorded graphs curve earlier and the sustained load goes down to zero earlier as seen in Figure 15. It is seen in Figure 16 that an inclined three-waves-long fiber presents a similar behavior to a two-waves-long fiber perpendicular in a 0.50 w/c ratio matrix, confirming in a certain sense the proposed mechanism of action. The bigger size of the cones reduces the anchored length so that an inclined fiber behaves like a shorter perpendicular fiber.

Statistical Analysis

A statistical analysis based on the analysis of variance (ANOVA) was performed to determine the significance of the effects measured for the following experimental responses (Figure 17) [20]:

- the load at the peak that corresponds to the maximum load that was supported by the fiber during its pull-out process;
- the displacement measured at this value of the load, called displacement at the peak load;
- the total energy developed during the pull-out process that corresponds to the area beneath the load-displacement curve. This last value was obtained by numerical integration.

DISPLACEMENT AT THE PEAK LOAD. Table 3 presents the values obtained for the displacement at the peak value for each of the 18 configurations.

Table 4 gives the result of the ANOVA of the values obtained for the displacement at the peak load value according to the procedure described in the Appendix.

It is clear from the last column of Table 4 that the length, the length-orientation interaction, and the orientation have been shown to have a statistical significant effect. It has been possible to check the validity of the statistical model by checking the independence of the residue (range between the predicted value by the model and actual value of the parameter) and the value given by the model [20].

Figure 18 illustrates the effect of the fiber length. Each point corresponds to the average of the values obtained for a given length. From a physical point of view, this significant effect can be interpreted by considering that the more the length of the fiber increases, the more the load increases. Therefore, the crushed cones will be bigger. This explains why the fiber is unfolded on a greater freed length at the peak load, which directly influences the displacement at the peak.

The same interpretation justifies the length-orientation interaction. The size of the cone increases when the length of the fiber increases and when the fiber departs from a 90° angle. This value could have been increased by the side effects observed in the cracked planes on our samples.

In conclusion, the overall mean peak displacement is 1.73 mm. This value is probably overestimated as a result of surface effect in the artificial cracked plane (Figure 19). However, this means that the mobilization of the fibers is not instantaneous and that the optimal ef-

TABLE 6. Analysis of variance on peak load values

Source	df	Sum of squares	Mean square	*F* value	*p* value
w/c	2	14155.444	7077.722	16.420	.0118
Length	2	498100.111	249050.056	577.768	.0001
Angle	1	125166.722	125166.722	290.373	.0001
w/c × length	4	94.222	23.556	.055	.9922
w/c × angle	2	36.778	18.389	.043	.9587
Length × angle	2	4776.778	2388.389	5.541	.0703
Residual	4	1724.222	431.056		

Dependent variable is peak load. *df* = degrees of freedom.

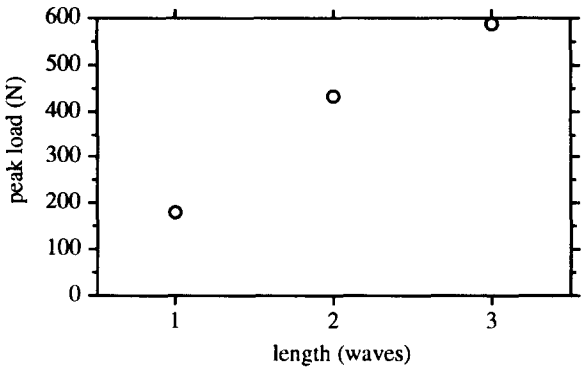

FIGURE 20. Influence of the fiber length on the peak load.

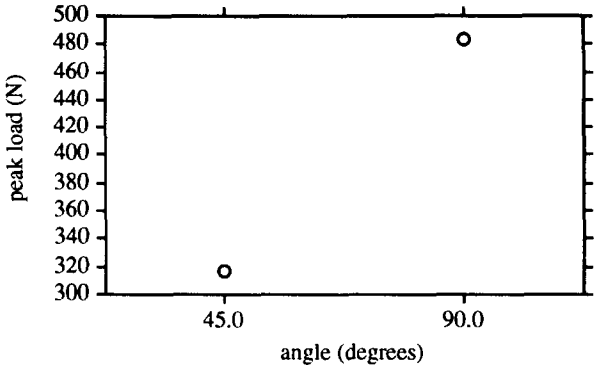

FIGURE 21. Influence of the fiber orientation on the peak load.

ficiency of the fibers may be obtained only after a given crack opening. This may explain the curve's shape in tensile or flexural tests on fiber-reinforced concrete depending on the fiber geometry [2,22].

LOAD AT THE PEAK VALUE. Table 5 presents the loads registered for each peak value for each of the 18 studied configurations. Table 6 analyzes the variance of the peak load. The significant effects are the length, the orientation, and the w/c ratio value.

As seen in Figure 20, the peak load increases with the fiber length, which is in good agreement with our knowledge of the fiber behavior. Moreover, the slope of the peak load decreases with increasing fiber length, which fits well with Bartos theory [23]. The asymptotic value is 660 N, which represents the ultimate load sustained by the fiber at failure.

Is is also clear that the peak load is more important when the fiber makes an angle of 90° rather than 45°, as seen in Figure 21. The size of the crushed cone being bigger at 45° reduces the anchored length of the fiber so that the load at the peak decreases.

ENERGY DISSIPATED DURING THE PULL-OUT PROCESS. Table 7 presents the energy dissipated during the pull-out process for each of the configurations studied, and Table 8 presents the ANOVA for this energy. The length, the orientation, the w/c ratio, and the length–orientation interaction have a significant effect on the energy dissipated.

The effect of the length of the fiber on the dissipated energy is presented in Figure 22. It is clearly seen in Figure 22 that when the length of the fiber increases, the dissipated energy increases. It seems that this energy does not vary linearly with the fiber length. It is interesting to note that this energy has been found to be a quadratic function of the fiber length in the case of straight fibers. The same type of relation has been obtained in the case of our corrugated fibers.

The other significant effects on the energy are already significant for the two previous parameters of the statistical analysis.

SYNTHESIS OF THE STATISTICAL ANALYSIS. Table 9 summarizes the significant effects for each parameter under study. It is seen that fiber length always plays a key role when studying the behavior of the fiber with respect to all parameters. It is the same for the orientation, which also interacts with the length.

The w/c ratio is not as important as other factors in this case. This is perhaps due to the way the samples were fabricated. In fact, the static position of the fibers during the fabrication of the specimens could have modified the actual nature of the fiber/matrix interface as compared with the nature of the interface when the fibers are energetically mixed within the concrete during the mixing process.

Finally, it has been seen that the nonlinear fiber under study developed a mechanical anchorage on top of the bonding mechanism. This last mode of anchorage induces a quite complex system of stress at the fiber/

TABLE 7. Energy dissipated (N.mm) during the pull-out process values

	45° angle			90° angle		
w/c	One wave	Two waves	Three waves	One wave	Two waves	Three waves
0.3	372	3056	7428	1094	4760	10382
0.5	269	1855	6478	550	4335	8709
0.7	236	1846	5101	463	3767	7457

TABLE 8. Analysis of variance on dissipated energy values

Source	df	Sum of squares	Mean square	*F* value	*p* value
w/c	2	5701909.778	2850954.889	35.734	.0028
Length	2	153427186.778	76713593.389	961.538	.0001
Angle	1	12294187.556	12294187.556	154.097	.0002
w/c × length	4	2669187.889	667296.972	8.364	.0318
w/c × angle	2	64225.778	32112.889	.403	.6930
Length × angle	2	3647580.111	1823790.056	22.860	.0065
Residual	4	319128.556	79782.139		

Dependent variable is fracture energy. *df* = degrees of freedom.

matrix interface that can modify our understanding of the role played by the w/c ratio on the global behavior of the fiber.

It is, therefore, important to limit to some extent the scope of this work due to the idealized conditions under which this experimental study was done. For example, the "perfection" of the precracked plane could favor the initial unfolding of the fiber following the observed crushing of small concrete cones. This phenomena could have altered slightly the shape of the peak on the load-displacement graphs. These points should be carefully analyzed when extending this model to describe the global behavior of the fiber-reinforced concrete.

Conclusion

During the experimental program presented here, two modes of failure of the fibers were observed. In one case, the fiber is broken; in the second case, the fiber debonds first, then slips in its print until it is finally pulled out. The lower the w/c ratio, the higher the failure load. However, in case of fiber debonding, the w/c ratio plays a minor role in the pull-out behavior of the fiber. This result has been confirmed by a statistical analysis that has shown that the length of the fiber and its orientation are major parameters, whereas the w/c ratio is a less significant parameter influencing the fiber matrix behavior.

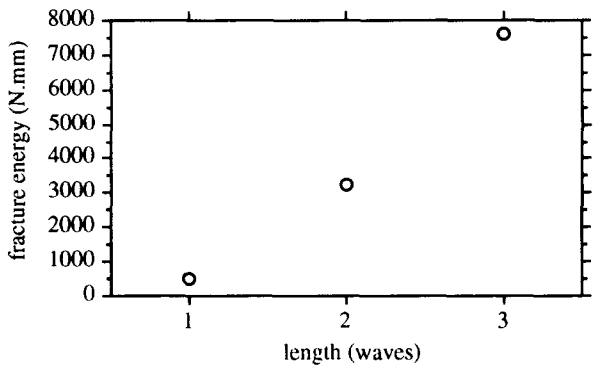

FIGURE 22. Influence of the fiber length on the dissipated energy.

Experimental observations pointed out that the failure process starts by the crushing of a small concrete cone on each side of the crack plane. The size of this cone varies with the configuration of the fiber matrix and greatly influences the behavior of fiber. In fact, it shortens the anchored length and allows the fiber to unfold on this freed length. This cone is more harmful on the properties of the composite when the fibers are inclined at a 45° angle.

Moreover, after their pull-out, the fibers are straightened so that they lose their initial shape. However, when observing in detail the aspect of the print after the total pull-out of the fiber, it is seen that only very minor degradations were developed along the print. This observation clearly indicates that the fiber slips within its initial print through continuous plastic deformation of each of its sections during the whole pull-out process. It is, therefore, the energy to create that cold working process that has to be developed during the pull-out of the fiber.

In conclusion, in spite of the two previously mentioned points (artificial crack, static fibers), it is the opinion of the authors that the experimental model under study led to a better understanding of the interaction between the particular fiber under study and the matrix that finally governed the global behavior of the composite. Such an approach, in addition to anisotropy of the fiber distribution and fiber group effects, may lead to an optimization of the properties of fiber-reinforced concrete.

TABLE 9. Synthesis of the statistical analysis

Parameter	Highly significant	Less significant
Peak load displacement	L; L × A	A
Peak load	L; A	w/c
Dissipated energy	L; A	w/c; L × A

L = length; A = angle.

Appendix

This appendix presents the statistical method used to analyze the variance of a factorial design. The statistical analysis of a set of data can be done in different ways. In the following, a simple but powerful method will be presented. It can be applied to what is called factorial design.

This method consists of choosing a certain number of parameters that could influence a particular behavior and, for each of these parameters, selecting a certain range of variation. As an example, in the present experimental study, the w/c ratio is one particular parameter for which we selected three values, 0.30, 0.50, and 0.70. Experimental results provide data for each possible configuration (combination of different levels for each parameter) with, in some cases, duplicates (more than one value for a particular configuration).

In the method used, only discrete values of the parameters were considered when studying their effect instead of continuous parameter. Moreover, the variance analysis was limited to the factorial design we selected. This factorial design had the three following parameters:

- w/c, the w/c ratio with three values, 0.30, 0.50, and 0.30;
- L, the length of the fibers with three values, 1, 2, and 3 waves; and
- A, the orientation of the fibers with two levels, 90° and 45°.

For each configuration, n duplicate values were obtained. In our case, n = 1 because we tested three specimens for each configuration. Only the mean response of these three specimens may be considered as independant duplicate.

Experimental data can be expressed by the following statistical linear model:

$$Y_{ijkl} = \mu + \tau_i + \beta_j + \gamma_k + (\tau\beta)_{ij} + (\tau\gamma)_{ik} + (\beta\gamma)_{jk} + (\tau\beta\gamma)_{ijk} + \varepsilon_{ijkl}$$

where Y_{ijkl} is the response (data) corresponding to the i^{th} level of w/c, the j^{th} level of L, the k^{th} level of A, and the l^{th} duplicate; μ is the responses overall mean; τ_i is the effect of the i^{th} level of w/c, i = 1.3; β_j is the effect of the j^{th} level of L, j = 1.3; γ_k is the effect of the k^{th} level of A, k = 1.2; $(\tau\beta)_{ij}$ is the effect of the interaction between w/c and L [the same for $(\tau\gamma)_{ik}$, $(\beta\gamma)_{jk}$, and $(\tau\beta\gamma)_{ijk}$]; and ε_{ijkl} is the error component.

With such a model, the effects of each parameter and of their interaction are defined according to the deviation they are bringing to the global average. To begin with, the direct effects of w/c, L, and A will be studied. More specifically, the equal influence of each configuration will be tested from a statistical point of view with our linear model. For example, for the factor w/c, this implies to test the following hypothesis:

$$\text{factor w/c:} \quad \begin{cases} H0 : \tau1 = \tau2 = \tau3 = 0 \\ H1 : \text{at least one } \tau i \neq 0 \end{cases}$$

Rejecting H0 means that the effect of the factor w/c is not zero, and so the factor w/c is a significant parameter. In addition, the different possible interactions between the parameters will also be studied.

To discuss this hypothesis, we will perform a statistical analysis of the variance. This means that the overall data variability will be split into different components. A measure of the overall variability is given by the following sum of square value:

$$SS_T = \sum_{i=1}^{3}\sum_{j=1}^{3}\sum_{k=1}^{3}\sum_{l=1}^{n}(Y_{ijkl} - \mu)^2$$

This sum of square values can also be rewritten as following where each term represents the sum of the square values due to a simple factor or due to the interaction of different factor. The term SS_E represents the sum of the square values related to the error. It is not our intention to provide the detailed calculations for each sum; they can be found in Montgomery [24]:

$$SS_T = SS_{E/C} + SS_L + SS_A + SS_{E/C \times L} + SS_{E/C \times A} + SS_{L \times A} + SS_{E/C \times L \times A} + SS_E$$

For each sum of square values, the following degrees of freedom (df) can be associated for a total n (3 × 3 × 2) − 1 = 18, n − 1 degrees of freedom (Table A1).

In the following, the mean square value for each effect is defined as the sum of the square values divided by the degree of freedom:

$$MS = SS/df$$

TABLE A1. Degrees of freedom (df) associated with all the effects

Source	w/c	L	A	w/c × L	w/c × A	L × A	W/c × L × A	error
df	2	2	1	4	2	2	4	18(n-1)

L = length; A= angle; df = degrees of freedom.

TABLE A2. Analysis of variance (ANOVA) table

Source of variation	Sums of squares	Degrees of freedom	Means squares	Ratio F0
w/c	$SS_{w/c}$	2	$MS_{w/c}$	$MS_{w/c}/MS_E$
L	SS_L	2	MS_L	MS_L/MS_E
A	SS_A	1	MS_A	MS_A/MS_E
w/c × L	$SS_{w/c \times L}$	4	$MS_{w/c \times L}$	$MS_{w/c \times L}/MS_E$
w/c × A	$SS_{L \times A}$	2	$MS_{L \times A}$	$MS_{L \times A}/MS_E$
L × A	$SS_{L \times A}$	2	$MS_{L \times A}$	$MS_{L \times A}/MS_E$
w/c × L × A	$SS_{w/c \times L \times A}$	4	$MS_{w/c \times L \times A}$	$MS_{w/c \times L \times A}/MS_E$
Error	SS_E	18 (n-1)	MS_E	
Total	SS_T	18n-1		

L = length; A = angle.

It is clear that if one parameter (or one interaction) has a significant effect, the mean square sum for this parameter will be greater than the mean square of the error. So, when comparing the value of the average square sum of a particular parameter to that of the error, it is possible to figure out if this parameter is significant. The table to study the analysis of the variance (ANOVA) can be figured as follows in Table A2.

It can be proved that if the linear model is adequate (if it includes the parameters and their interactions that can be significant) and if appropriate hypothesis on the error e_{ijk} are made (normality hypothesis), each value for F0 is distributed according a Fisher law with the degree of freedom respectively associated to the source of variation (*d*) and to the error (*de*).

So, to test the hypothesis related to the significance of the various parameters, the ratio F0 of the ANOVA has to be compared to the Fisher coefficient $F\alpha,d,de$ where α is the level of significance (probability to reject the hypothesis H0 when it is true). The hypothesis H0 can be rejected if: $F0 > F\alpha,d,de$. It can be then immediately concluded that the studied parameter plays a significant role on the result with a degree of significance α.

In our experiment, only a single replicate is available per configuration, the average value obtained from the three specimens tested. In such a case, the error sum of square may not be estimable. Consequently, a plausible model to be assumed is that the higher level interaction mean square is not significant and may be confounded with the error mean square:

$$MS_E = MS_{W/C \times L \times A}$$

Table A3 shows the ANOVA, and the significance of the various effects can be made again on the basis of the Fisher test as previously described.

References

1. *State of the Art Report on Fiber Reinforced Concrete, Concrete International.* American Concrete Institute, 4 Detroit, MI: 1982; pp 9–30.
2. Rossi, P.; Acker, P.; Malier, Y. *Materials and Structures* **1987,** *20,* 436–439.
3. Bartos, P. *Int. J. Cem. Comp. Lightweight Concr.* **1981,** *3,* 1–18.
4. Gray, R.J. *J. Mater. Sci.* **1984,** *19,* 861–870.
5. Lawrence, P. *J. Mater. Sci.* **1972,** *7,* 1–7.
6. Brandt, A.M. *J. Mater. Sci.* **1985,** *20,* 3831–3841.
7. Gopalaratnam, V.S.; Jin-Cheng. In *Material Research Society Symposium Proceedings 114;* Materials Research Society: Pittsburgh, 1987; pp 225–232.
8. Naaman, A.E.; Namur, G.; Najm, H.; Alwan, J. *Bond Mechanisms in Fiber Reinforced Cement-Based Composites,* UMCE 89-9; University of Michigan: Ann Arbor, 1989; p 233.
9. Potrzebowski, J. In *Proceedings of the Third International Symposium;* Warsaw, Poland, 1991; pp 352–361.
10. Morton, J.; Groves, G.W. *J. Mater. Sci.* **1974,** *9,* 1436–1445.
11. Naaman, A.E.; Shah, S.P. *Am. Soc. Civil Eng. Proc.* **1976,** *102,* 1537–1549.
12. Banthia, N. *Can. J. Civil Eng.* **1990,** *17,* 610–620.

TABLE A3. Analysis of variance (ANOVA) table

Source of variation	Sums of squares	Degrees of freedom	Means squares	Ratio F0
w/c	$SS_{w/c}$	2	$MS_{w/c}$	$MS_{w/c}/MS_E$
L	SS_L	2	MS_L	MS_L/MS_E
A	SS_A	1	MS_A	MS_A/MS_E
w/c × L	$SS_{w/c \times L}$	4	$MS_{w/c \times L}$	$MS_{w/c \times L}/MS_E$
w/c × A	$SS_{L \times A}$	2	$MS_{L \times A}$	$MS_{L \times A}/MS_E$
L × A	$SS_{L \times A}$	2	$MS_{L \times A}$	$MS_{L \times A}/MS_E$
Error		4	MS_E	
Total	SS_T	17		

13. Stroeven, P. *Heron* **1979,** *24,* 7–40.
14. Hughes, B.P.; Fattuhi, N.I. *Mag. Concr. Res.* **1975,** *27,* 161–166.
15. Maage, M. *Materials and Structures* **1977,** *10,* 297–301.
16. Bartos, P. *J. Mater. Sci.* **1980,** *15,* 3122–3128.
17. Gopalaratnam, V.S.; Abu-Mathkour, H.J. *Proceedings of the International Symposium on Fiber Reinforced Concrete,* vol. 2; Madras, India, 1987; pp 201–211.
18. Gokoz, U.N.; Naaman, A.E. *Int. J. Cem. Comp.* **1981,** *3,* 187–202.
19. Chanvillard, G. *Réunion Scientifique des groupements de recherches coordonnées;* Greco Geomateriaux, CNRS: Toulon, France, 1990; p 14.
20. Chanvillard, G. *Analyse expérimentale et modélisation micromécanique du comportement des fibers d'acier tréfilées, ancrées dans une matrice cimentaire.* Thesis, University of Sherbrooke: Canada, 1992.
21. Banthia, N.; Trottier, J.-F.; Pigeon, M.; Krishnadev, M.R. In *High Performance Fiber Reinforced Cement Composites;* Reinhardt, H.W.; Naaman, A.E., Eds.; E&FN Spon: London, 1992; pp 456–466.
22. Chanvillard, G.; Banthia, N.; Aïtcin, P.-C. *Cem. Concr. Comp.* **1990,** *12,* 41–46.
23. Bartos, P. *J. Mater. Sci.* **1980,** *15,* 3122–3128.
24. Montgomery, D.C. *Design and Analysis of Experiments;* John Wiley & Sons: New York, 1984; p 518.